

# Time expansion chamber for characterization of TWIST low energy muon beams

J. Hu<sup>a</sup>, G. Sheer<sup>a</sup>, Yu.I. Davydov<sup>a,b</sup>, D.R. Gill<sup>a</sup>,  
P. Gumplinger<sup>a</sup>, R.S. Henderson<sup>a</sup>, B. Jamieson<sup>a</sup>, C. Lindsay<sup>a</sup>,  
G.M. Marshall<sup>a</sup>, K. Olchanski<sup>a</sup>, A. Olin<sup>a</sup>, R. Openshaw<sup>a</sup>,  
V. Selivanov<sup>b</sup>

<sup>a</sup>TRIUMF, Vancouver, BC, V6T 2A3, Canada

<sup>b</sup>RRC "Kurchatov Institute", Moscow, 123182, Russia

---

## Abstract

A low mass time expansion chamber (TEC) has been developed to measure distributions of position and angle of the TRIUMF low energy surface muon beam used for the TWIST experiment. The experiment is a high precision measurement of muon decay and is dominated by systematic uncertainties, including the stability, reproducibility, and characterization of the beam. The distributions measured by the TEC are one essential ingredient of an accurate simulation of TWIST. The uncertainties, which are extracted through comparisons of data and simulation, must be known to assess potential systematic uncertainties of the TWIST results. The design criteria, construction, alignment, calibration, and operation of the TEC are discussed, including experiences from initial beam studies. A brief description of the use of TEC data in the TWIST simulation is also included.

Key words: Drift chamber, Time expansion chamber, Low energy muon beams  
PACS: 29.40.Gx, 14.60.Ef, 13.35.Bv

---

---

Corresponding author. Address: TRIUMF, 4004 Wesbrook Mall, Vancouver, BC V6T 2A3, Canada. Tel: 604-222-7466. Fax: 604-222-1074. Email: glen.marshall@triumf.ca.

## 1 Introduction

The TRIUMF Weak Interaction Symmetry Test (TWIST) measures momentum and angle distributions of positrons from the decay of highly polarized positive muons, to determine precisely the decay ("Michel" [1,2,3]) parameters. It uses a solenoidal spectrometer with 2 T magnetic field consisting of 56 planar drift and proportional chambers arranged symmetrically with high precision on either side of a central foil that stops the low energy muon beam [4]. The incident polarized muon beam is directed along the axis of the solenoid from the beam line, through the fringe field region, and into the chamber stack within the uniform tracking region. Following the decay of the muon, the positron is tracked in the chambers and a high statistics decay distribution is acquired. The first results from the experiment have been published [5,6]. To extend those results to higher precision, and especially to analyze and assess systematic uncertainties for the polarization dependent asymmetry decay parameter  $P$  [7], a method was required to measure quickly and reliably the muon beam characteristics near the entrance to the solenoid. While the TWIST detector itself, especially the first several planes of drift chambers, has some excellent properties for this kind of measurement, its placement is disadvantageous. It is located after materials that contribute to multiple scattering, such as a vacuum window and trigger scintillator. In addition, the gas density at atmospheric pressure and the extra cathode layers of the first detector chambers add intolerable scattering sources.

### 1.1 Muon beam polarization

The requirements of high polarization and rapidly achieved high statistics are satisfied by a beam of surface muons [8] produced at the surface of the primary proton target from pion decay at rest. High polarization with respect to the direction of momentum  $\hat{p}$  ( $P^p$ , which is exactly 1 if the Standard Model holds true) is assured, because the helicity of the muon neutrino determines the spin angular momentum of the recoiling muon. The resulting particles have momentum of 29.79 MeV/c and a range of only 0.15 g cm<sup>-2</sup> in carbon. Those that are created within the primary target, some distance from its surface, will lose energy and undergo multiple scattering prior to escaping into the surrounding vacuum. Some scattering can also occur in a removable polyester gas barrier window in the beam line, of thickness 2 mm; it is used with graphite targets to isolate emitted radioactive isotopes which would otherwise migrate to the spectrometer. Scattering reduces the correlation of momentum and spin directions, and thus the polarization, so it is essential to select only those muons near the maximum momentum allowed in the decay to keep this depolarization at a level negligible compared to the sensitivity of the TWIST

measurements.

If this goal is achieved, the muons transported to the end of the beam line by magnetic elements will retain the correlation of momentum and spin direction,  $P^{\parallel}$ . The ensemble polarization of the beam with respect to a beam axis  $\hat{z}$ ,  $P^z$ , will be less than  $P^{\parallel}$  for a beam of finite emittance, but no other significant depolarizing interactions intervene.

As the muon passes from the beam line through the solenoid fringe field and into the tracking region, the momentum and spin direction retain their correlation ( $P^{\parallel}$  is preserved), but transverse momentum components are added in the fringe field and an apparent depolarization with respect to the solenoid (and beam) axis is the result, i.e.,  $P^z$  decreases. This can be modeled quite precisely in simulations, assuming the field shape is known sufficiently well, and also assuming the particle positions and momenta can be determined for some point near the entrance to the field.

A device to measure the beam particle positions and momentum directions has been constructed, on the principles of the Time Expansion Chamber (TEC) [9]. It determines the track of an ionizing particle in one dimension, transverse to the particle's direction, via the drift time of ionization in a relatively uniform drift field. The ionization then reaches a region of higher field where gas amplification takes place near a sense wire anode. Because we require beam characteristics in both dimensions (x and y) transverse to the beam direction (z), the TWIST TEC consists of two orthogonal modules.

## 2 Design, construction, and operation

Surface muons are easily scattered, so to minimize multiple scattering effects, the primary design criterion for the TWIST TEC was to maintain low mass. The detector must also operate in the vacuum of the muon beam channel, which in this case is not isolated from the primary production target nor from the accelerator itself. Operation of the detector using low pressure dimethyl ether (DME) gas allows the use of thin windows that isolate the chamber gas from the beam line vacuum. DME, having a long drift time, small Lorentz angle, and high primary ionization, is convenient because it is also used for TWIST drift chambers. An automated control system ensures that this low differential pressure is maintained. The overall length of the TEC was kept to a minimum compatible with a reasonable track length necessary for an accurate direction measurement. The beam size can range up to a few centimeters, so a somewhat larger active area was chosen, within which the only materials in the beam path are the entrance and exit windows, the low pressure chamber gas, and very thin field cage wires required to define the drift field.

The typical muon rate for TW IST measurements is up to several thousand per second, so the device must be capable of recording such rates. Its operation should also not be compromised by typical beam contaminants such as positrons. Even though the TEC material in the beam path has been minimized, it scatters the beam too much to be used simultaneously during some of TW IST's high precision muon decay measurements. The primary role of the TEC is to periodically tune and measure beam characteristics, verify stability, and detect possible changes in the beam that may have occurred in a measurement interval during which it was removed to acquire precise muon decay data. Therefore, another important design feature was that the detector can be installed into and removed from the beam line quickly, conveniently, and reproducibly.

## 2.1 Design of the TEC

The TEC is located directly upstream of the TW IST spectrometer and is attached to the end of the TRIUMF M13 beam line [10] as shown in Fig. 1. The beam passes from the final two quadrupoles through a gate valve and into the TEC. It then continues in vacuum through the fringe field near the yoke end plate until it reaches a vacuum window inside the high field region. From there, it passes through a variable density gas degrader, a thin trigger scintillator, and into the TW IST detector.

As can be seen in Fig. 2, the TEC consists of two identical modules rotated 90 degrees with respect to each other and mounted in an aluminum gas box. One module tracks the horizontal (x) position and angle of the incoming muons and the other the corresponding vertical (y) components. Each module is 80 mm long. The active area that can be measured by the TEC is 60 mm  $\times$  60 mm transverse to the beam, with an active length of 48 mm (24 wires spaced by 2 mm). The gas box has 6 mm aluminumized Mylar entrance and exit windows and is nested in a vacuum box. The flow of DME gas is maintained in the gas box at a pressure of 80 mbar.

Figure 3 shows an exploded three-dimensional rendering of a TEC module. The sense and grid planes are nominally 1.6 mm thick G-10 (epoxy/glass) printed circuit boards (PCB's) as are the side walls of the field defining cage. The drift field planes are 3.2 mm thick PCB's. The remaining structural elements of the module are also manufactured from G-10. The connectors have gold plated contacts in a glass-filled polyester matrix. The module is assembled with nylon cap screws. All materials have been tested for compatibility with the DME gas [11].

Each module contains a drift field region and gas amplification region. The

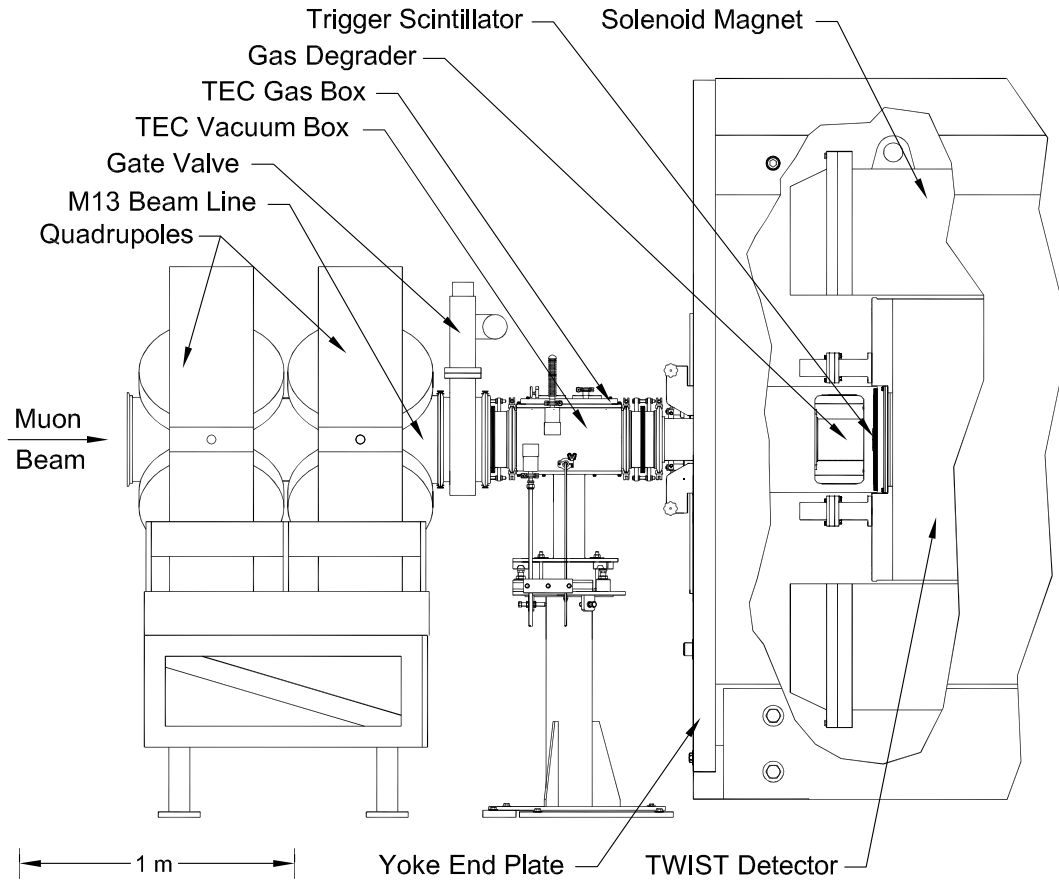


Fig. 1. Placement of the TEC in the muon beam between the exit of the beam line and the TWIST solenoid.

former consists of a four sided field defining cage with two wall elements containing parallel printed circuit traces and two field planes with 50  $\mu\text{m}$  gold plated Cu/Be wires strung across the opening. The wires of the field plane are electrically connected to the side wall traces through gold plated pins and a socket assembly. The pitch of the wires and traces is 2.54 mm. To achieve a uniform electric field, each group of wires and traces is connected to its neighbor through resistors of the same value creating a resistor chain to which high voltage is applied. The drift cathode plane on the bottom of the field cage is a copper plane on a 1.6 mm G-10 substrate.

The gas amplification region consists of a grid wire plane, a sense wire plane and a solid cathode plane. These planes are separated by spacer planes made of 1.6 mm G-10. A section of the wire geometry of this configuration is shown in Fig. 4. The grid and shield wires are 125  $\mu\text{m}$  gold plated Cu/Be. The sense wires are 25  $\mu\text{m}$  gold plated tungsten. The signals from the 24 sense wires are taken from the end of the PCB through a coaxial cable assembly to a feedthrough in the gas box lid.

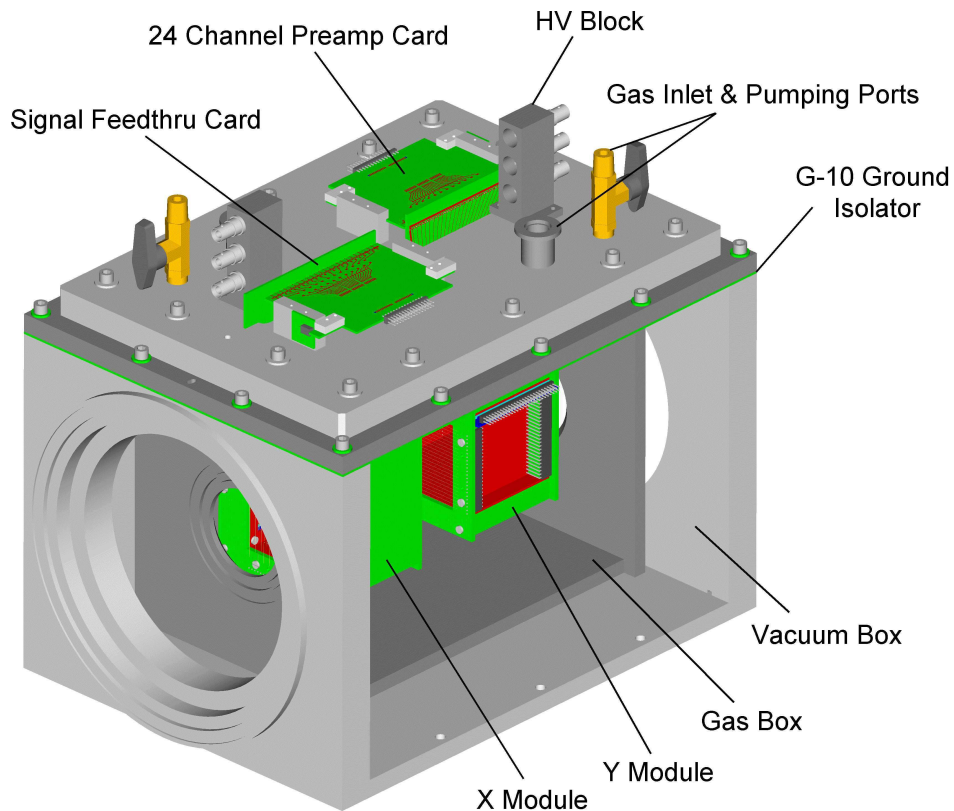


Fig. 2. TEC modules in the gas box.

When the elements of the drift field region and gas amplification region are mated, the last resistor in the field defining cage is connected to the grid plane, which is maintained at ground potential as is the ground plane on the other side of the sense plane. As shown in Fig. 4, the sense plane is made up of alternating sense and shield wires. Gas gain only occurs at the thinner sense wires. The diameter of 25  $\mu$ m was chosen for these wires based on our previous study of gas gain at low pressure [12]. The shield wires screen the induced pulses from adjacent wires and are necessary because the average angle of the muon tracks through the TEC is quite small. This results in signals on adjacent sense wires occurring at very nearly the same time, so the mutually induced pulses would seriously affect the rise time of these signals and hence the accuracy of the drift time measurement.

## 2.2 TEC Alignment

It is important to align the TEC very accurately with respect to the TWIST spectrometer and hence with the measured field map. Cross-hairs were mounted in the apertures at each end of the steel yoke of the spectrometer to define the z axis. An optical surveying instrument (theodolite) was then used to align

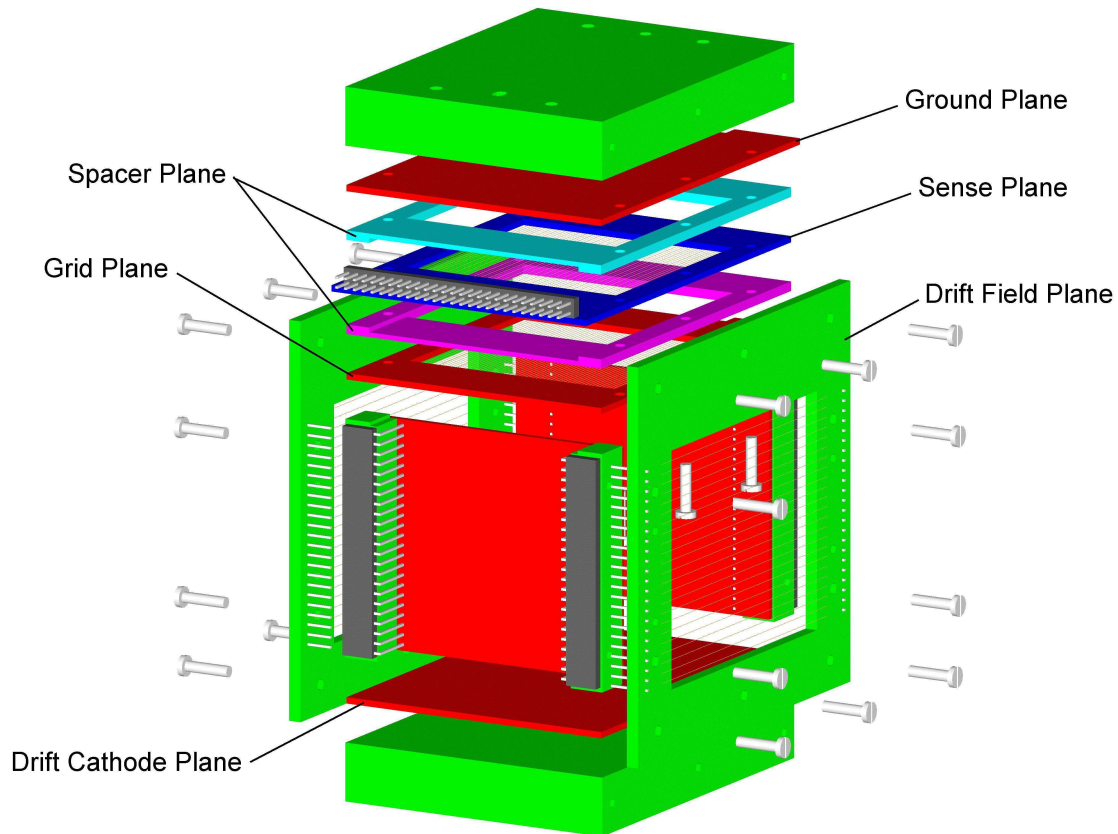


Fig. 3. Exploded three-dimensional view of one TEC module.

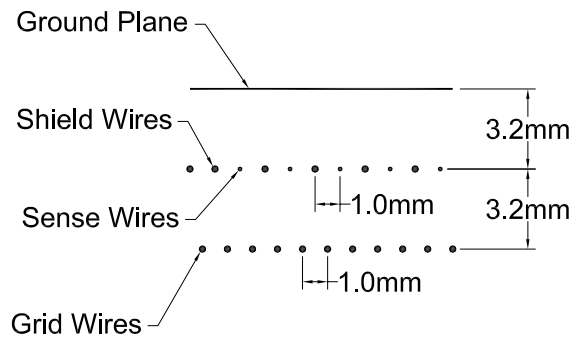


Fig. 4. Sense plane geometry.

the TEC to these cross-hairs. First the x and y positions of the TEC were adjusted to align the field cage wires for both x and y modules, and then the location was checked with the position of the central hole of the calibration collimators (see Sec. 3.2). The accuracy was approximately 250  $\mu$ m. Once this alignment was completed another optical device, a Leica TDA 5005 Total Station, was used to record the position of the TEC with respect to the M13 beam line and TWIST spectrometer.

The TEC gas box has been design to be removed and replaced in a very reproducible manner using locating pins in the vacuum box. However, any time the TEC is removed and replaced, a measurement of its position is made with the Total Station to confirm that proper alignment has been maintained. The accuracy of this measurement is  $\pm 50 \mu\text{m}$ . It was necessary to take precautions to avoid movement due to forces from vacuum loading of the beam line and magnetic fields of the solenoid.

### 2.3 TEC operation

The optimum drift field for the TEC was found to be approximately  $16 \text{ V/m}$ . The applied sense wire high voltage is  $1150 \text{ V}$  and the shield wires are at  $300 \text{ V}$ . These voltages result in a muon track efficiency of essentially 100% with typically up to 19 out of 24 wires hit per muon track (see 3.3). There are intermittent sparks, the location and cause of which are still undetermined. A degradation of efficiency over a period of weeks of operation has also been observed, which may be a result of the sparking. Although the origins of these effects are not yet understood, the practical solution of regular replacement of sense wire planes has been adopted.

### 2.4 Electronics and readout

The 24 wires of each of the TEC modules are connected to 24 channel preamplifiers mounted on the lid of the TEC gas box. The preamplifiers were developed at Fermilab for use at their Colliding Detector Facility [13]. Each channel has a gain of  $1 \text{ mV/fC}$  and a dynamic range of  $-400 \text{ fC}$  to  $+20 \text{ fC}$ . Signals are taken via  $9.5 \text{ m}$  of micro-coaxial cable to custom made post-amplifier/discriminator modules, which have sixteen channels in a single width CAMAC module and are also used in the readout of the TWIST spectrometer [4]. The resulting discriminated ECL logic signals are then sent via  $15 \text{ m}$  of twisted pair cable to a LeCroy 1877 FASTBUS TDC. These TDC's are multihit type, have  $0.5 \text{ ns}$  resolution and are operated in common stop mode. The trigger signal for the TDC's is derived from a plastic scintillator mounted downstream of the TEC.

### 2.5 Gas system

The TEC gas system is required to provide a flow (typ.  $100 \text{ cc/min}$ ) of DME to the TEC while maintaining a constant pressure (typ.  $80 \text{ mbar}$ ) in the TEC.

Upstream pressure control is accomplished with an absolute pressure transducer that measures the pressure in the TEC volume. This transducer signal is fed to a proportional-integral-differential (PID) device controlling the flow through a mass flow controller in the gas supply line to the TEC. Downstream flow control is provided by a manual precision needle valve in the exhaust line between the TEC and the exhaust pump. The observed pressure control stability, as reported by the pressure transducer, is approximately 0.1%. The manufacturer's specifications for the pressure transducer indicate an absolute accuracy (combined linearity, hysteresis and non repeatability) of 0.25% and a temperature drift of 0.048% = C at the typical operating pressure.

DME is a flammable gas and it is separated from the cyclotron vacuum by thin 6 mm windows. Consequently, major design features of the gas system include interlocks and procedures to prevent differential pressure from rupturing the 6 mm windows and to avoid flammable mixtures of air and DME in the TEC. To provide redundancy, an independent bipolar differential pressure transducer is used to monitor continuously the differential pressure across the windows. A programmable logic controller is used to read the various pressure, flow and other status inputs and implement the interlock logic. The system has three modes of operation; TEC\_Out, Pump/Vent, and Normal Operation.

The TEC\_Out mode is used when the TEC has been removed from the vacuum box. Whether or not the TEC is in the vacuum box is detected by a microswitch on the vacuum box mating flange. In this mode, all the TEC supply and exhaust valves are forced closed, thus isolating the gas system. High voltage to the TEC is disabled. The control system's only active functions are to control in a safe way the gate valve separating the TEC vacuum box from the beam line, and the valve connecting the vacuum box to its vacuum pump and vent ports, with interlocks based on the pressures reported by vacuum gauges in the TEC vacuum box and the beam line.

In the Pump/Vent mode, some valves are forced open, while others are forced closed, such that the TEC and all of the connecting supply and exhaust tubing, which can be at sub-atmospheric pressure during normal operation, can be pumped out through a bypass valve connecting the TEC to the TEC vacuum box. This ensures that possible air leaks into the TEC or any of its connecting plumbing can be discovered. The gate valve is forced closed in this mode, isolating the TEC vacuum box from the beam line during vent and pump down procedures. High voltage to the TEC is disabled. The bypass valve connecting the TEC to the vacuum box can be closed to assist in locating leaks. However, it is forced open if the differential pressure across the windows exceeds a set point limit.

The Normal Operation mode has the most complex interlock scheme. The bypass valve and the valve connecting the vacuum box to the vent and vacuum

pump ports cannot be opened. The TEC high voltage is enabled only if all the valves in the gas supply and exhaust lines are open and the DME flow to the TEC exceeds a set point limit (typ. 30 cc/min). The gate valve can be open only if the vacuum box and beam line pressures are satisfactory and the differential pressure across the TEC windows is below a first set point limit. The gas system valves in the DME supply and exhaust lines can be open only if the vacuum box pressure is satisfactory, and the differential pressure across the windows is below the first set point limit. If despite being isolated from the gas system, the magnitude of the differential pressure continues to increase beyond a second, higher set point limit, the bypass valve connecting the TEC to the vacuum box is forced open to relieve the pressure across the windows. This second limit is set at 160 mbar, well below the 500 mbar typically required to rupture the windows.

### 3 Calibration and Tracking

#### 3.1 Field distortion

The field cage is used to produce a uniform drift field for electron clusters. Ideally, the field along the drift direction is constant,  $E = 1000 = 60.96 = 16.4$  V/mm everywhere in the drift volume. In reality, however, the field distribution is distorted because of the high voltage applied on the sense plane and the electric field penetrating from the adjacent module. The FEM LAB Program [14] was employed to study such effects. Figure 5, from the simulation of a single module, shows that the drift field at the center of the drift volume (i.e., at  $x = 0$  for the X module) changes by about 10% over the length of the module with the sense plane turned on (open squares), and a clear curve is visible. Compared with the nominal -16.4 V/mm value, the field intensity is enhanced near the middle. When the sense plane is turned off (open circles), the field is reduced everywhere, such that the value near the middle is approximately the nominal value. This indicates that the grid plane is not completely effective in shielding the drift region from the sense plane potential, but there is still a curvature in the shape of the field even without the sense plane effect. This is likely due to influence of the field cage. In a test with FEM LAB, the grid plane was extended to cover the gap between the edge of the grid plane and the field cage, and the field cage wires were replaced with aluminumized Mylar strips. The edge effects are then reduced significantly. With the sense plane off, the drift field is nearly constant across the module (filled triangles). Because the aluminumized Mylar strips introduce more multiple scattering into the beam, they were not used in the actual TEC. Instead, field variations were accounted for via the position-dependent calibration procedure described in the next section.

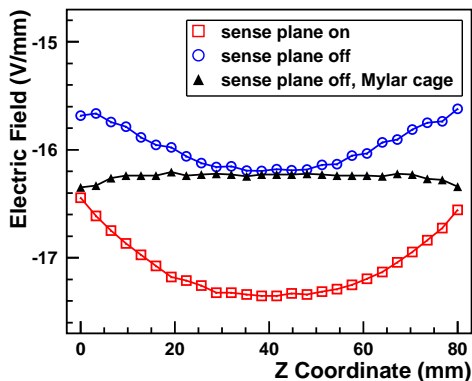


Fig. 5. Calculated drift field at the center ( $x = y = 0$ ) of a single module. Sense wire plane on and off are shown to demonstrate the effect on the dominant field. The active region, where the sense wires are located, is from  $z = 17$  mm to  $z = 63$  mm.

Another source of field distortion comes from interference between the two modules. Figure 6 is a contour plot of the change of field in the drift region of the X module when the Y module is turned on. This could bias the beam angle measurements by up to roughly 5 mrad even though the interference effect is on the order of 1%.

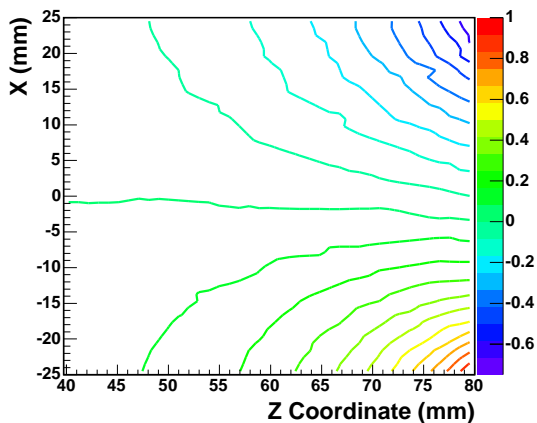


Fig. 6. Contours of calculated electric field contribution in the X module at  $y = 0$ , due to field leakage from the Y module. Color-coded contours show the field change in percentage of the nominal central field (16.4 V/mm) of the X module. The difference in the x component of the field, when the Y module is turned on, is plotted in the portion of the drift region of the X module nearest the Y module.

### 3.2 Extraction of space-time relationship

Precise characterization of the muon beam requires an adequate space-time relationship (STR) for a TEC cell, which is defined by two neighboring shield and grid wires with a sense wire in the middle. As discussed in the previous section, the electric field in the drift region is not uniform. The drift velocity varies with the drift distance and the z position of the sense wire. A pair of multi-hole collimators, installed 141 mm upstream and downstream with respect to the center of the TEC gas box, is used as an external reference system to measure the STR as a function of various operating parameters. Each collimator, as shown in Fig. 7, consists of a square array of 7 × 7 holes, 1.2 mm in diameter, separated by 5.00 mm. The positions of holes were measured to an accuracy better than 40 μm. Calibration data were taken with a diuse beam tune so that all holes have exposure from the beam. We selected the beam tracks with an angle near zero mrad for calibration purposes. An example of a projection of measured positions from one row of the collimator array is shown in Fig. 8.

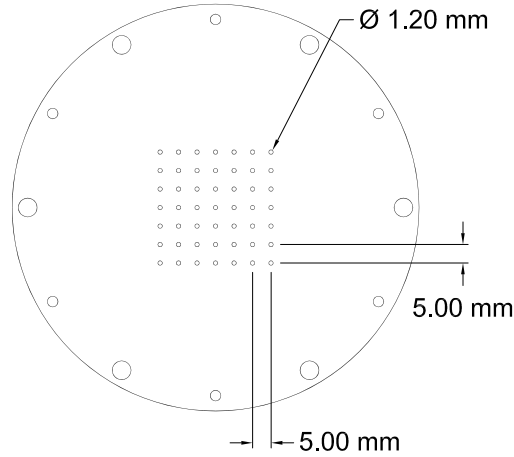


Fig. 7. A schematic plot of a collimator. One is placed at each end of the TEC gas box to define tracks to be used for calibration.

A third order polynomial function was used to fit the STR :

$$d_{ij}^k = p_0^k + p_1^k t_{ij}^k + p_2^k (t_{ij}^k)^2 + p_3^k (t_{ij}^k)^3$$

(k = 1; ;48; and i; j = 1; ;7)

where  $d_{ij}^k$  is the distance between the  $k^{\text{th}}$  sense wire and the hole in the  $i^{\text{th}}$  row and the  $j^{\text{th}}$  column;  $t_{ij}^k$  is the corresponding mean drift time. Figure 9 presents an example of the fit quality. The cubic term reduces residuals by 10{20% ; higher order terms were found to be negligible. With d in cm and t in s, the linear term is of order one, while the quadratic and cubic terms are of order

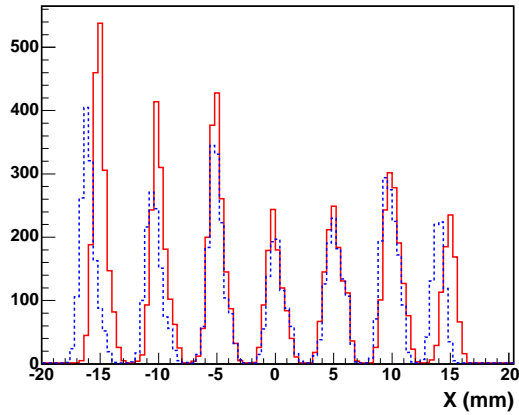


Fig. 8. Projection in  $x$  of measurements for particles passing through holes in one row of the collimator prior to calibration (blue dotted line, based on GARFIELD without field leakage) and following calibration (solid red line).

$10^{-2}$  and  $10^{-3}$  respectively. The drift times for particles in the active area of the TEC are typically up to 8 ns.

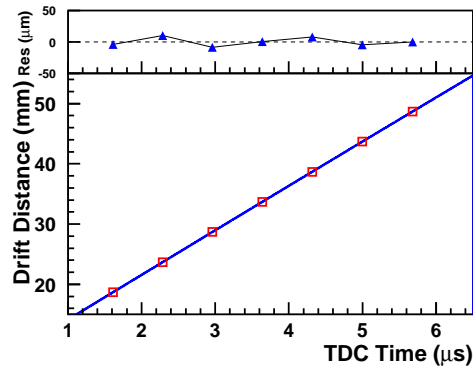


Fig. 9. Fit of the drift distance to the uncorrected TDC time to derive the STR. The plot at the top of the figure gives the residual of the fit.

While the calibration procedure has been shown to be quite adequate for the central active area of the TEC ( $30 \times 30 \text{ mm}^2$ ) corresponding to the collimators described above, it is likely that the derived STR is not as accurate at the extremities. Collimators that cover the entire active region will be used in the future.

Simulations with GARFIELD [15] suggest that the drift time has an almost linear relationship with temperature and therefore gas density (as illustrated at a field of  $16.4 \text{ V/mm}$  in Fig. 10). Data taken at  $22^\circ\text{C}$  and  $25^\circ\text{C}$  confirm the temperature dependence. Because the DM E gas pressure is fixed at 80 mbar and the temperature is recorded by the data acquisition system, variations of

the STR with the gas density have been taken into account either by taking the calibration data under the same temperature or by linearly rescaling the STR according to the density.

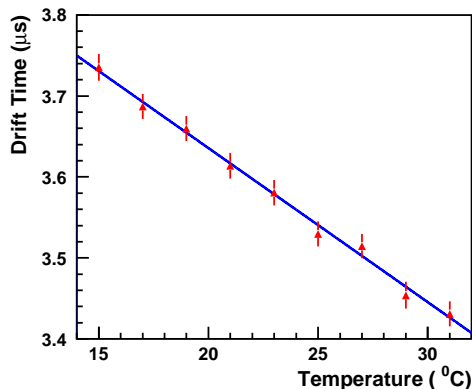


Fig. 10. Drift time variation with DME gas temperature. Plotted are drift times predicted by GARFIELD at a field of 16.4 V/mm for a muon track on the TEC central axis for various gas temperatures.

### 3.3 Tracking resolution

The trigger for readout of an event in the TEC is provided by a signal from a plastic scintillator placed after it. Associated with the trigger within a time window of some 10 ns, one, or rarely more than one, muon may pass through the TEC. Minimum ionizing positrons are also present in the beam, but are detected only with very low efficiency in the low gas density. In fact, even muons above 50 MeV/c are not tracked efficiently with 80 mbar pressure. Regardless of the source, multiparticle (multitrack) events are rejected from the analysis. In the tracking code, track candidate signals are identified from different wires within the time window. The drift time is determined with respect to the trigger scintillator time, and the drift distance is derived by converting from drift time with the help of the STR. The drift distance, or transverse track position, is fit versus the z position with a straight line. The straight line is found to be a good approximation even though the solenoid fringe field extends to the TEC position, where it is typically about 0.1 T and mostly in the z direction.

There are three major contributions to the resolution of the chamber: the spread of drift times in a TEC cell, the multiple scattering effect, and diffusion of the electron clusters. Due to the TEC geometry, drift times within the same cell can vary significantly. Figure 11, obtained from a GARFIELD study for drift field of 16.4 V/mm, shows the variation of drift time versus z position of

ionization. A variation of up to 2% can be seen for an average drift distance, equivalent to 75 ns or about 0.6 mm .

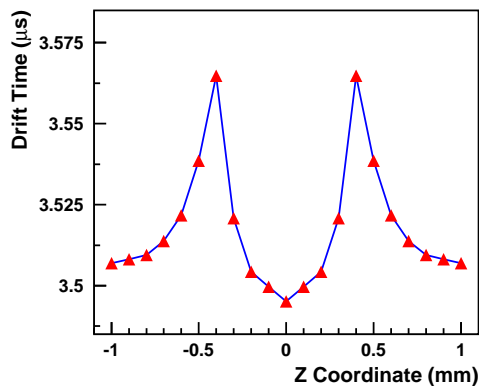


Fig. 11. Dependence of the drift time on  $z$ , from a GARFIELD study with drift field 16.4 V/m for a muon track on the central axis.  $z = 0$  mm corresponds to the location of the sense wire and  $z = \pm 1$  mm to the adjacent shield wires, while grid wires are at  $z = \pm 0.5$  mm .

The spatial resolution of an individual TEC cell is determined by fitting the tracks without including hits from that cell and then measuring the residuals. It ranges from 150 to 350  $\mu$ m, as a function of distance from the sense wire, getting worse with increasing drift distance as shown in Fig. 12. The dependence of hit resolution on drift distance is probably caused by transverse and longitudinal diffusion of electron clusters. The longer the drift, the less likely is the cluster to exceed electronic threshold due to the fact that diffusion separates the electrons in the cluster. On average, when there are 18 wires hit in a track, the track angle resolution is 3 mrad while the position resolution, when extrapolated to a plane midway between the two TEC modules, is 150  $\mu$ m .

As discussed in Sec. 2.3, while the tracking efficiency is essentially 100% , the hit efficiency is not. Figure 13 is a distribution of the total number of wires hit (of a maximum possible of 24 wires in a module) for a track as a function of drift distance, where the inefficiency due to the longer drift is clearly visible. Except for this distance correlation, the absence of a hit on a wire seems to occur randomly along the length of the track.

#### 4 Characterization of the TWIST beam

After alignment and calibration, it is possible to obtain and analyze distributions of positions and angles, and to measure correlations between them , in

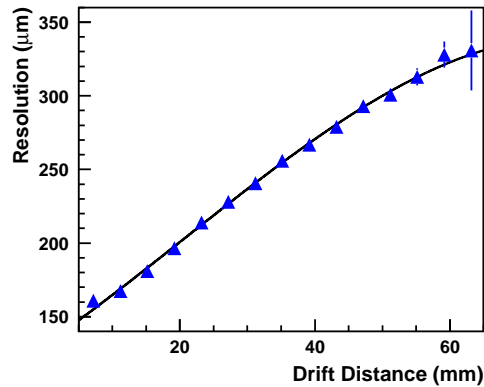


Fig. 12. Measured resolution as a function of track distance from the sense wire.

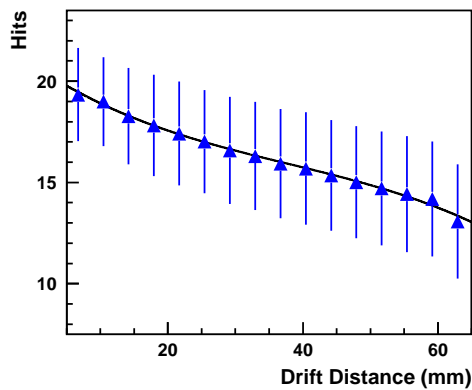


Fig. 13. Total number of valid hits as a function of track distance from the sense wire. Error bars represent widths of the hit number distribution.

a very brief time. This section describes typical measurements and how they are used by the TWIST group to adjust the beam and to analyze muon decay data.

#### 4.1 TEC measurements and implications for TWIST

The objectives for beam quality for TWIST were established early in the planning of the experiment. Simulations of a muon beam entering the solenoidal field showed that, to achieve the required small depolarization of order  $10^{-3}$ , the beam should have an rms size of about 5 mm and rms angle of about 15 mrad in the absence of solenoid field, at a position near the field fringe where radial field components are highest when the solenoid is on. Therefore, the

calibration and resolution uncertainties of the TEC must be small compared to these values.

Extensive beam studies based on TEC data with the solenoid field resulted in beam characteristics that satisfied the requirements. The short beam measurement time necessary for a precise measure of means and widths of size and angle distributions, as well as indications of asymmetry or unusual beam shape, allowed many different beam tests and adjustments. The effects of slits, apertures, and absorbers in the M13 beam were observed and settings were optimized. Quadrupole steering was minimized, and beam stability over days and weeks was tested. Two surface muon production targets were used in the studies. The first was an edge-cooled graphite surface muon production target of 10 mm length. The second was a beryllium target of 12 mm length encased in a stainless steel water cooling jacket; it produced an asymmetric x profile some 20% larger than the graphite, thus it is considered inferior for TWIST muon decay measurements.

When the solenoid was turned on to its full 2 T central field, and correct calibration of the TEC was verified, it was observed that the incoming muon beam was steered to positive values of  $x$  and  $y$ . Figure 14 shows an  $xy$  beam image with these conditions, from a graphite production target. Note that the intrinsic beam size, without the TEC, is somewhat smaller than implied by the figure, because some of the multiple scattering produced by the TEC occurs prior to tracking in the TEC modules. While the solenoid fringe field does not appreciably alter the beam size, the shift of position away from the solenoid axis, believed to be due to the interaction of the solenoid fringe field with beam quadrupoles and the main beam dipole, is a cause for concern. It reduces the polarization with respect to the solenoid axis ( $P^z$ ), such that it is less likely to be simulated with the high absolute precision required by TWIST. Steering in the beam line to compensate for the fringe field effect is being implemented for future TWIST measurements.

## 4.2 Use of TEC data in TWIST simulations

The Monte Carlo simulation of each TWIST event begins with the generation of an input muon. Other beam particles (muons and positrons) are also generated, randomly correlated in time according to measured rates, to simulate the real beam environment. The muon beam distribution in position and angle that is input to this simulation is derived from the TEC measured particle tracks extrapolated to a  $z$  position corresponding to the middle of the TEC. At this location, multiple scattering has an adequately small effect on the transverse ( $xy$ ) profile. The angular distributions then contain most of the influence of scattering, and can be modified to account for it to some level of

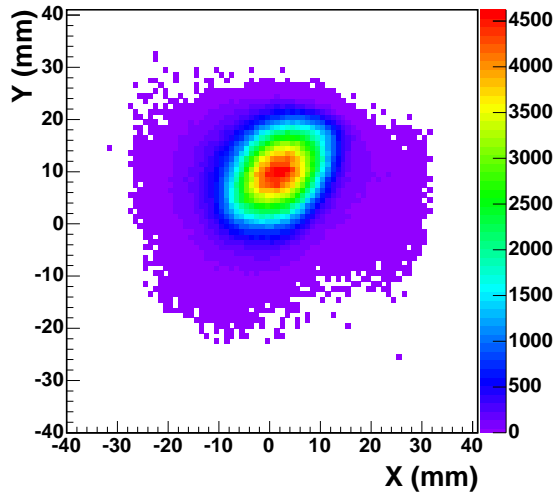


Fig. 14. Two-dimensional distribution of the muon beam intensity at the TEC, near the fringe field region of the TWIST spectrometer. The pixel size in the figure is  $1 \times 1 \text{ mm}^2$ .

precision by a deconvolution procedure.

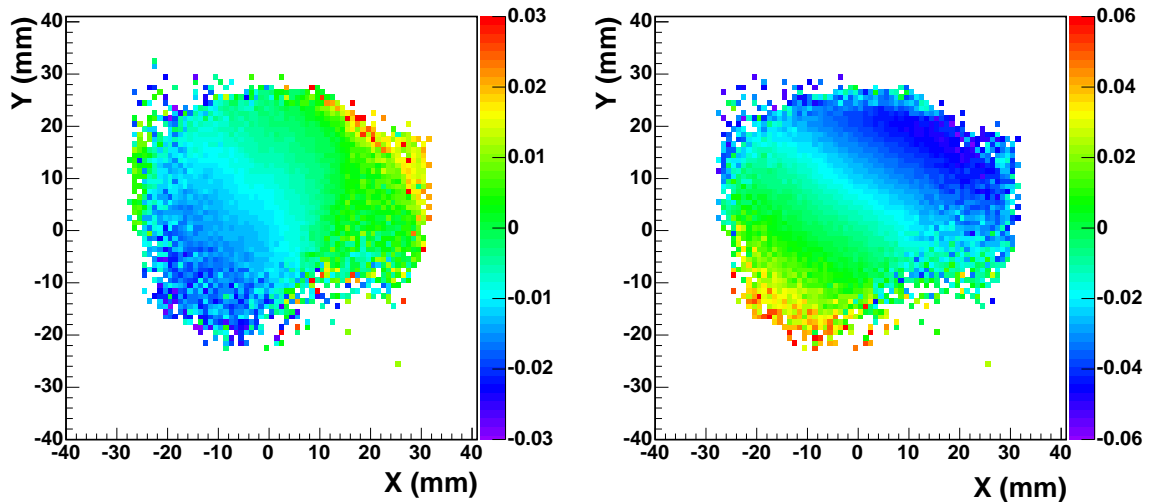


Fig. 15. Two-dimensional distributions of the muon beam mean angle projected to the  $y = 0$  plane ( $x$ , left) and to the  $x = 0$  plane ( $y$ , right) for the beam intensity distribution shown in Fig. 14. Note that the color scales, representing the angles in radians, are different to show the trends more clearly.

Deconvolution of the angular distributions is carried out in the simulation. The inputs to the simulation are: the probability of a muon at each  $xy$  position as derived from a two-dimensional distribution such as Fig. 14, the mean angles of the muon in  $x$  ( $x$ ) and  $y$  ( $y$ ) for each  $xy$  position as shown in Fig. 15, and the rms of the angle distributions for each  $xy$  position. The simulation generates an  $xy$  transverse location according to the probability of Fig. 14, using an array

with elements of  $1 \text{ mm}^2$  as shown in the figures. Random Gaussian numbers are generated with mean given by the values of  $x$  and  $y$  at the  $xy$  point as in Fig. 15. The figure shows the rotation of the angle-position correlation due to the fringe field of the solenoid, and the smaller divergence of the beam in the  $x$  direction than in  $y$ , for this particular beam tune. The corresponding rms widths used for the random numbers at each  $xy$  point are also taken from the TEC information. However, they must be reduced compared to the measured values, to account for the scattering added by the materials of the TEC as the particle passes through it; this is the deconvolution. This technique is intended to reproduce the correlations found between the angles,  $\theta_x$  and  $\theta_y$ , and the positions,  $x$  and  $y$ . Correlations between  $\theta_x$  and  $\theta_y$  have been observed to be very small and are not simulated.

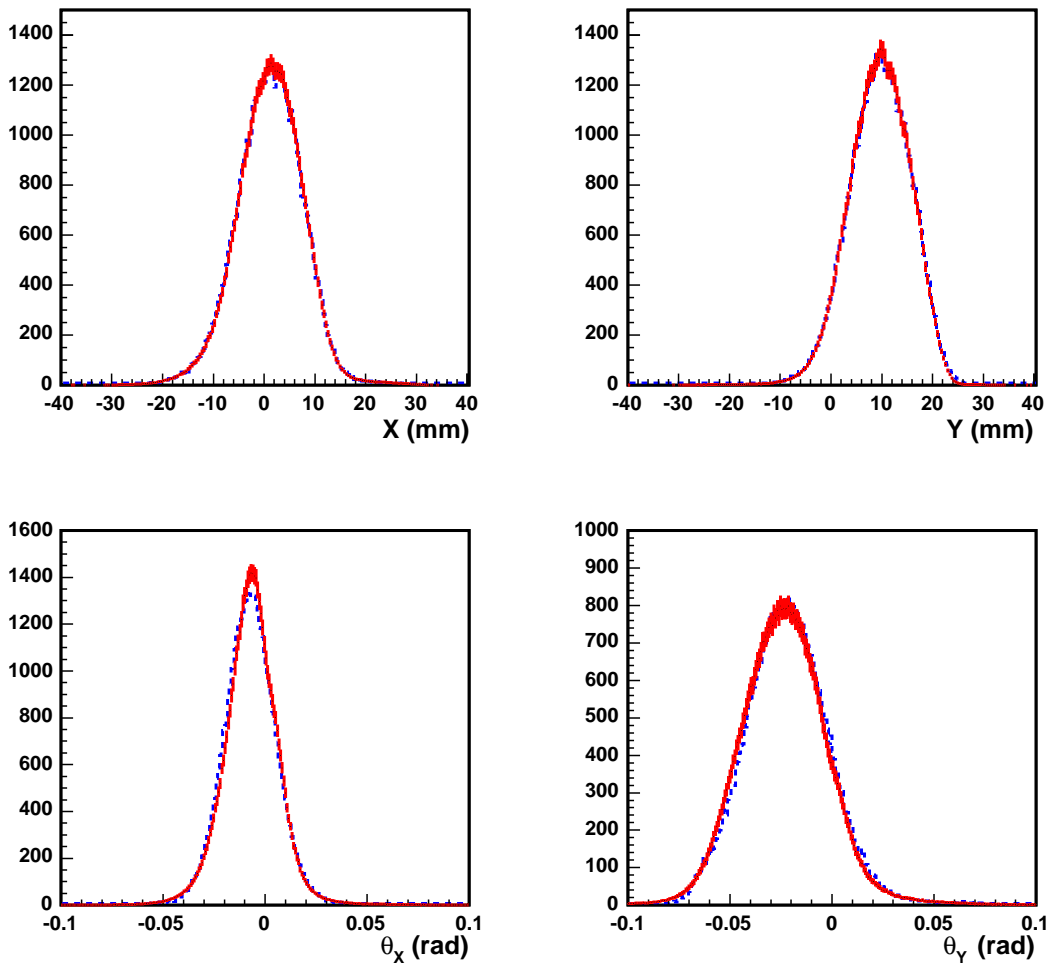


Fig. 16. Distributions in positions and angles of a beam as measured (solid red lines) and as simulated following the deconvolution procedure (dashed blue lines).

Projections of real measured positions and angles are shown in Fig. 16, along with a comparison from a similar analysis of TEC data produced by a sim -

ulation that uses a correlated deconvolution of the real distributions as an input. The muon is scattered by the TEC entrance window ( $2.1 \times 10^5$  radiation lengths) and by 3.5 cm of DME gas ( $1.3 \times 10^5$  radiation lengths) before it reaches the TEC X module, resulting in a smearing of the measured  $\sigma_x$ . Scattering has an even larger influence on the  $\sigma_y$  measurement as the muon travels through another 12.0 cm of DME ( $4.6 \times 10^5$  radiation lengths) before it reaches the Y module. The effect of smearing due to scattering is compensated by reducing each angle distribution width (deconvoluting) at an average scattering position along the particle path. The deconvolution widths are derived from comparisons of reconstructed TEC tracks from simulation runs with the multiple scattering turned off and turned on. The values corresponding to the analysis of recent data were 9.5 mrad for  $\sigma_x$  and 12.6 mrad for  $\sigma_y$ , which are subtracted quadratically from the measured widths for each xy location. When the distribution of angles for the entire beam is plotted, including this contribution from multiple scattering, the lower two panes of Fig. 16 show a 12.4 mrad rms width of  $\sigma_x$  and a 20.1 mrad rms width of  $\sigma_y$ .

## 5 Summary

The TEC has already provided TWIST with extremely important information about the muon beams used to make high precision measurements of muon decay as a test of the Standard Model. In the future, we expect to be able to improve the optimization of beam characteristics (beam size and divergence) to provide the minimum possible depolarization of the beam as it enters the solenoidal field of the spectrometer. We will also be able to determine what factors affect the muon beam, and by how much. This in turn will enable us to minimize systematic effects of the muon decay parameter determinations caused by variations in the muon beam, and also to assess accurately the influence of residual systematics. Finally, data from the TEC will be crucial to a reliable simulation of the muon beam, which in turn will be necessary for the detailed simulation of all aspects of the experiment. Because the extraction of muon decay parameters from data depends on a high precision comparison to the simulation, the success of the experiment ultimately will depend in part on the data supplied by the TEC.

We acknowledge with gratitude the assistance of P. Bennett, S. Chan, L. Ellstrom, B. Evans, and M. Goyette, as well as the entire TWIST collaboration. TEC construction and development was supported by TRIUMF and the National Research Council of Canada. TWIST is supported by research grants from the National Sciences and Engineering Research Council of Canada, by the US DOE, and by the Russian Ministry of Science.

## References

- [1] L. Michel, Proc. Phys. Soc. A 63 (1950) 514.
- [2] C. Bouchiat, L. Michel, Phys. Rev. 106 (1957) 170.
- [3] A. Sirlin, Phys. Rev. 108 (1957) 844.
- [4] R. L. Henderson, et al., Nucl. Instr. and Meth. A 548 (2005) 306.
- [5] TWIST Collaboration, J. R. Musser, et al., Phys. Rev. Lett. 94 (2005) 101805.
- [6] TWIST Collaboration, A. Gaponenko, et al., Phys. Rev. D 71 (2005) 071101 (R).
- [7] TWIST Collaboration, B. Jamieson, et al., in preparation (2006).
- [8] A. Pifer, T. Bowen, K. Kendall, Nucl. Instr. and Meth. 135 (1976) 39.
- [9] A. H. Walenta, IEEE Trans. Nucl. Sci. NS-26.1 (1979) 73.
- [10] C. J. Oram, et al., Nucl. Instr. and Meth. 179 (1981) 95.
- [11] R. Openshaw, R. Henderson, Nucl. Instr. and Meth. A 515 (2003) 89.
- [12] Y. I. Davydov, et al., Nucl. Instr. and Meth. A 545 (2005) 194.
- [13] R. J. Yaremka, et al., IEEE Trans. on Nucl. Sci. NS-39 (1992) 742.
- [14] <http://www.femlab.com/products/multiphysics>.
- [15] R. Veenhof, GARFIELD, A Drift-Chamber Simulation Program, User's guide, ver 7.04, CERN (2001).